electronics

MDPI

Article

Robust EEG Watermark via Dual-Stream Frequency–Time Attention Network Against Signal Processing Attacks

Lei Zhang, Weicheng Zhou, Tianyu Ding, Chaoen Xiao *, Jianxin Wang, Ding Ding and Jiao Lei

Department of Electronic and Communication Engineering, Beijing Electronic Science and Technology Institute, Beijing 100070, China; zhanglei@besti.edu.cn (L.Z.); 20253905@mail.besti.edu.cn (W.Z.); 20253821@mail.besti.edu.cn (T.D.); wangjianxin@besti.edu.cn (J.W.); dingding@besti.edu.cn (D.D.); 20253919@mail.besti.edu.cn (J.L.)

* Correspondence: xce@besti.edu.cn

Abstract

Digital watermarking secures electroencephalogram (EEG) data in distributed Brain–Computer Interface (BCI) environments. However, existing single-domain deep learning schemes struggle to maintain robustness against clinical signal processing attacks due to EEG's joint time–frequency nature. We introduce the Dual-Stream Frequency–Time Attention Network (DS-FTAN), utilizing an adaptive Spectral Gating Mechanism to embed information within robust, high-energy EEG spectral regions. A robustness simulation layer—encompassing resampling, spectral dropout, and band-pass filtering—is incorporated during training. Validations confirm DS-FTAN balances imperceptibility (PSNR $>$ 36 dB) with reliable recovery. Specifically, it achieves $>$99.99% accuracy under no-attack conditions and maintains 86.52–98.77% accuracy across complex attacks (e.g., 50% cropping, band-pass filtering). This significantly outperforms time-domain baselines. Furthermore, DS-FTAN exhibits excellent zero-shot cross-channel generalization. It preserves diagnostic integrity, causing merely a 0.42% accuracy drop in downstream EEGNet intention recognition. Ultimately, this framework provides a reliable solution for privacy-preserving EEG data sharing.

Keywords: biomedical signal processing; EEG; digital watermarking; deep learning; dual-stream attention; spectral gating; robustness

1. Introduction

In recent years, with the rapid evolution of Brain–Computer Interface (BCI) technology and remote medical monitoring systems [1], the electroencephalogram (EEG) as a physiological signal objectively reflecting neural activity has been widely adopted in clinical diagnosis, rehabilitation engineering, and affective computing [2]. While conventional cryptographic techniques are designed to ensure data confidentiality [3,4], digital watermarking technology is predominantly employed for tracking and traceability verification [5,6]. By imperceptibly embedding copyright or authentication information directly into the raw EEG data [7,8], it enables persistent tracking and provenance verification even in open data-sharing environments. However, EEG watermarking poses more stringent challenges than other multimedia data. First, EEG signals are characterized by weak microvolt-level voltages, non-stationarity, and a low signal-to-noise ratio. Consequently, even minuscule embedding perturbations can obscure critical pathological features (e.g., epileptic spikes), potentially causing clinical misdiagnoses [9,10]. Second, routine clinical preprocessing

Check for updates

Academic Editor: Subir Halder

Received: 15 May 2026
Revised: 20 June 2026
Accepted: 24 June 2026
Published: 1 July 2026

Copyright: © 2026 by the authors. Licensee MDPI, Basel, Switzerland. This article is an open access article distributed under the terms and conditions of the Creative Commons Attribution (CC BY) license.

such as band-pass filtering, downsampling, and denoising to remove power-line or EMG artifacts acts as signal processing attacks. These inevitable procedures threaten watermark integrity, demanding high algorithmic robustness [11,12].

Numerous researchers have focused on image watermarking and proposed a variety of effective schemes [13,14]. In recent years, with the rise of deep learning, researchers have leveraged its powerful feature learning and non-linear modeling capabilities to develop advanced watermarking systems capable of resisting complex attacks; for instance, one study significantly enhanced watermark robustness against transformations like rotation and scaling by introducing a noise layer that simulates geometric attacks within the HiDDeN architecture [15,16]. The DARI-Mark scheme proposed by Zhao et al. [17] utilizes a deep learning and attention network to significantly enhance watermark robustness. Wang et al. [18] achieved a better balance between watermark robustness and imperceptibility by introducing an adaptive strength factor. The Edit-guard study by Zhang et al. [19] demonstrated the versatility of watermarking technology in both tamper localization and copyright protection. Concurrently, several reversible data hiding schemes for medical signal security have been proposed in the medical field, where data integrity is paramount [20]. Against this technological backdrop, the applications of digital watermarking continue to expand, and consequently, it has emerged as a pivotal technology for EEG copyright confirmation and traceability, particularly in burgeoning fields of brain science research and clinical applications.

With breakthroughs in deep neural networks for generative tasks, deep learning-based EEG watermarking has become a focal point of research. Qin et al. [21] proposed the RPW-EEG framework, which employs a two-stage end-to-end training strategy. By enhancing robustness via a multifunctional noise layer and recovering task-related features through adversarial fine-tuning, this method effectively balances copyright protection with downstream task utility, achieving high imperceptibility with a Peak Signal-to-Noise Ratio (PSNR) of 25.26 dB. However, its watermark extraction accuracy currently hovers around 61% under various attack scenarios, indicating that maintaining robust protection in complex practical environments remains a significant challenge. The fundamental reason for this vulnerability is that most existing deep watermarking models (including RPW-EEG) are directly adapted from Convolutional Neural Network (CNN) architectures used in computer vision, treating EEG merely as one-dimensional time-series data. This simplistic transfer overlooks the intrinsic spectral characteristics and physiological rhythm distribution of EEG signals. Specifically, pure convolution architectures are constrained by local receptive fields and struggle to capture global frequency-dependent relationships, rendering the generated watermarked signals fragile against frequency-domain operations, such as mandatory band-pass filtering. Consequently, when subjected to clinical filtering attacks, the bit error rate of existing deep learning models often rises sharply, failing to meet the robustness requirements of practical scenarios.

To address these significant limitations in current methodologies, this paper proposes a novel EEG watermarking framework termed the Dual-Stream Frequency–Time Attention Network (DS-FTAN). Unlike previous methods that focus solely on time-domain features, DS-FTAN introduces a synergistic frequency–time processing mechanism designed to capture multi-domain dependencies. We design a parallel dual-stream module that utilizes the Fast Fourier Transform (FFT) to explicitly extract the spectral distribution of the signal and employs an adaptive Spectral Gating Mechanism to precisely identify and leverage frequency bands that remain highly robust under aggressive filtering attacks for information embedding. Furthermore, to significantly enhance the model's generalization capabilities across diverse scenarios, we construct a comprehensive robustness simulation strategy encompassing physical resampling, spectral dropout, and band-pass filtering constraints,

thereby incorporating complex real-world signal processing attacks directly into the training loop. Experimental results show that this method achieves an extraction accuracy of over 99.99% with high imperceptibility (PSNR $>$ 36 dB). Notably, the model exhibits significant robustness against a variety of intensive attack scenarios, including 50% signal cropping, severe Gaussian noise, and aggressive band-pass filtering. Moreover, the watermarking process strictly preserves the original physiological characteristics, causing a negligible performance degradation in downstream BCI tasks.

The main contributions of this paper are summarized as follows:

- We propose a novel Dual-Stream Frequency–Time Attention Network (DS-FTAN) for EEG watermarking. By introducing an adaptive Spectral Gating Mechanism, this architecture effectively overcomes the inherent blind spots of traditional CNNs in capturing EEG spectral characteristics.
- We design a hybrid robustness simulation strategy incorporating band-pass constraints, physical resampling, and spectral dropout tailored to the physiological nature of EEG signals. This not only significantly improves the model's survivability under intensive signal processing attacks but also endows it with zero-shot cross-channel generalization capabilities.
- Experiments validate that DS-FTAN achieves a balance between imperceptibility (PSNR $>$ 36 dB) and robustness. Crucially, it strictly preserves the diagnostic utility for downstream BCI classification tasks, providing a viable, plug-and-play security solution for distributed EEG data sharing.

2. Methods

2.1. Model Overview

The EEG watermarking task is fundamentally a constrained end-to-end signal reconstruction problem. We utilize the original single-channel or multi-channel EEG signal as the host carrier, while the secret information to be embedded consists of a 32-bit binary bit stream. Our objective is to learn a pair of non-linear mapping functions: the Encoder and the Extractor.

As illustrated in Figure 1, the DS-FTAN framework comprises three tightly coupled components. First, the Encoder is responsible for transforming discrete binary information into continuous micro-perturbations. These perturbations are adaptively superimposed onto specific time–frequency regions of the carrier EEG to generate the watermarked signal. To simulate realistic and hostile transmission environments, we embed a Robustness Simulation Layer within the training loop. Positioned between the Encoder and the Extractor, this layer functions as a hybrid data augmentation module incorporating fully differentiable operations. It subjects the watermarked signal to a variety of attacks, including noise interference, spectral truncation, and resampling. Finally, the Extractor receives the potentially corrupted signal and reconstructs the original binary sequence through deep feature decoding. The entire system is trained in an end-to-end manner by jointly optimizing signal reconstruction quality and information decoding accuracy.

2.2. Dual-Stream Frequency–Time Attention Block

To address CNNs' local limitations and frequency-domain blind spots, we propose the DS-FTAN Module, which captures complementary time–frequency features via a dual-stream parallel architecture. As illustrated in Figure 2, in the operational flow of this module, input features are first split into two parallel paths. The Time-Domain Path aims to capture the morphological features of EEG signals, such as transient spikes and the positional information of peaks and troughs. We employ a one-dimensional convolutional

layer coupled with Batch Normalization and the SiLU activation function to extract deep temporal representations while maintaining temporal resolution.

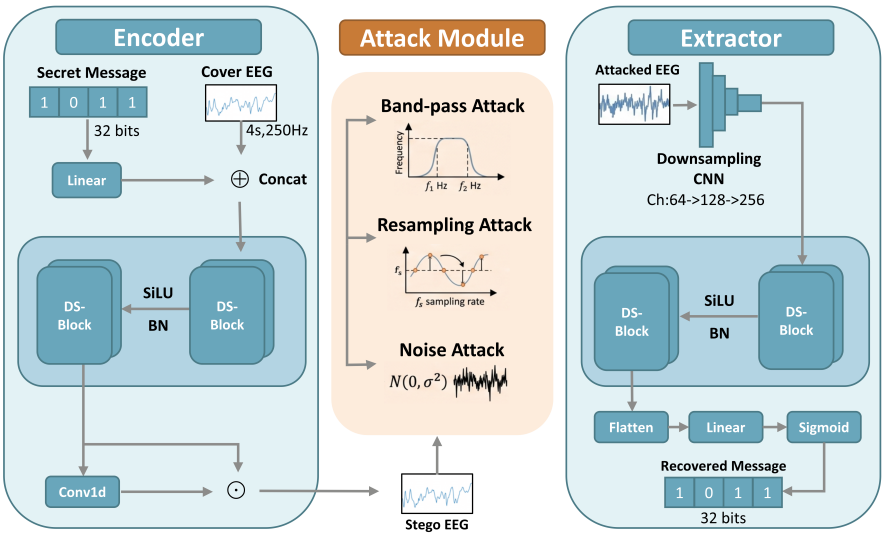

Figure 1. DS-FTAN Model Overview.

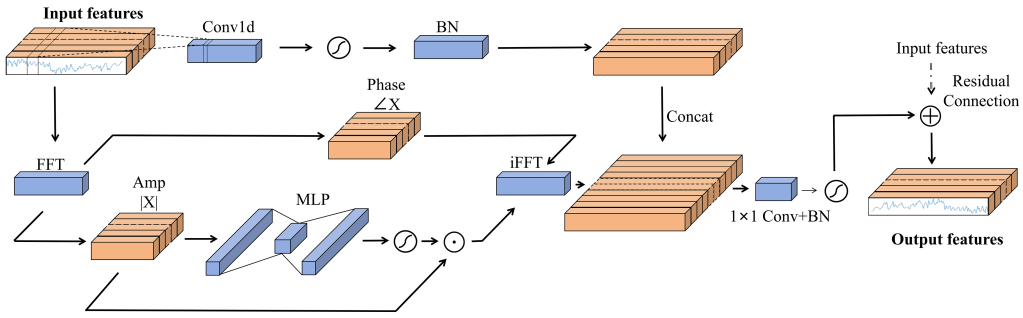

Figure 2. The Structure of Dual-Stream Frequency–Time Attention Block.

Simultaneously, the Frequency-Domain Gating Path explicitly processes the spectral characteristics of the signal. While advanced time–frequency distributions, such as the Choi–Williams transform [22], have demonstrated strong capability in analyzing non-stationary physiological signals by effectively suppressing cross-term interferences, adapting them for deep learning-based generative tasks remains challenging. Therefore, to ensure strict mathematical invertibility and computational efficiency required for end-to-end watermark reconstruction, our framework employs the real-valued Fast Fourier Transform (RFFT) paired with a parallel time-domain convolutional path to capture spatiotemporal dynamics. To empower the model with the ability to adaptively select robust frequency bands, we designed a magnitude-based Spectral Gating Mechanism. To extract physically meaningful representations, the resulting complex spectrum is explicitly decoupled into a magnitude spectrum, denoted as A, and a phase spectrum, denoted as Φ. Specifically, the magnitude spectrum A is derived by computing the absolute value of the complex RFFT output. Given an input temporal feature sequence of length L, the dimension of the resulting magnitude spectrum A strictly maps to $L/2+1$. We then employ a Multi-Layer Perceptron (MLP) to perform a non-linear transformation directly on the magnitude spectrum to learn and generate a global frequency mask. To maintain maximum frequency resolution and capture cross-frequency dependencies, the MLP is architected with two fully connected linear layers without dimensionality reduction. Both linear layers maintain a constant hidden dimension equal to the input size ($L/2+1$). A ReLU activation is applied after the first

linear layer, and the final output is normalized via a Sigmoid function (σ) to ensure the gating weights are strictly bounded between 0 and 1. This global mask is then used to weight the original magnitude spectrum:

$$G = \sigma(W_2 \cdot \mathrm{ReLU}(W_1 \cdot A + b_1) + b_2) \tag{1}$$

$$F_{freq} = \mathrm{iFFT}(A \odot G, \Phi) \tag{2}$$

where $\odot$ denotes the Hadamard product and W_1, b_1, W_2, b_2 represent the learnable weights and biases of the two linear layers, respectively. It is crucial to highlight the distinction between this proposed Spectral Gating Mechanism and existing frequency-domain attention or adaptive filtering techniques. Traditional adaptive filters often rely on predefined mathematical heuristics or static parameters, making them rigid when facing unpredictable clinical noises. Conversely, conventional deep learning attention mechanisms primarily focus on spatial or channel-wise dependencies, neglecting the intrinsic spectral distribution of EEG signals. In contrast, our mechanism is entirely data-driven and optimized end-to-end with the primary watermarking task. Physically, this process acts as a dynamic, soft band-pass filter, enabling the model to automatically identify and redundantly embed information within high-energy physiological bands that are inherently resilient to attacks (e.g., clinical band-pass filtering), while suppressing frequency components susceptible to noise interference.

Subsequently, the gated frequency-domain magnitude is recombined with the original phase spectrum Φ, reverted to the time domain via the inverse real-valued Fast Fourier Transform (iFFT) and concatenated with the features extracted from the temporal path along the channel dimension. Specifically, both the temporal features F_{time} and the frequency features F_{freq} possess an identical number of hidden channels, denoted as C. Upon concatenation, the resulting multi-modal feature map expands to $2C$ channels. To adaptively fuse these complementary representations while preserving the original temporal resolution, we employ a 1×1 one-dimensional convolutional layer (with a kernel size of 1 and a stride of 1) to project the $2C$ channels back to C channels. Furthermore, a residual connection is introduced to mitigate the gradient vanishing problem inherent in deep networks, thereby ensuring the smooth propagation of the feature flow:

$$Y = X + \mathrm{Conv}\left(\left[F_{time}, F_{freq}\right]\right) \tag{3}$$

2.3. Network Architecture Details

Building upon the aforementioned DS-FTAN module, we construct asymmetric architectures for the Encoder and Extractor to accommodate their distinct task requirements.

The Encoder adopts a lightweight U-Net style design, aimed at embedding information rapidly and imperceptibly. First, the secret information S is expanded via fully connected layers to match the temporal dimension of the EEG signal and is subsequently concatenated with the original host carrier signal along the channel dimension. This hybrid input undergoes deep feature transformation through a series of stacked DS-FTAN modules, layer-by-layer encoding the discrete information into continuous feature maps. To strictly limit the distortion imposed by the watermark on the original EEG waveform, the output layer of the Encoder does not directly predict the watermarked signal; instead, it predicts an additive residual. We employ a Tanh activation function to constrain the output within the range of $[-1, 1]$ and introduce a learnable scaling factor α to globally constrain the perturbation magnitude. The final generated watermarked signal can be expressed as:

$$C_{stego} = C + \alpha \times \mathrm{Tanh}\left(\Phi_{enc}\left(F_{deep}\right)\right) \tag{4}$$

This residual generation strategy ensures that the watermark energy is consistently maintained within a low range, thereby maximally preserving the time-domain waveform characteristics of the original EEG.

The Extractor employs a deep discriminative architecture. To retrieve faint watermark features from noisy signals, the front-end network utilizes a series of convolutional layers with a stride of 2 to progressively downsample the input signal. This process not only expands the effective receptive field of the neurons but also effectively filters out high-frequency noise interference. Subsequently, the compressed feature sequence enters a backbone network composed of multiple layers of DS-FTAN modules. Here, the spectral gating mechanism once again plays a critical role, assisting the Extractor in distinguishing valid watermark signals from background EEG noise or external attack interference. Finally, the feature vectors are flattened and mapped back to the binary space via fully connected layers to complete the information decoding.

2.4. Robustness Simulation Strategy

A primary challenge facing deep learning-based watermarking models in practical deployment is the domain shift, where clean training data fails to encapsulate the complex signal processing operations encountered in real-world scenarios. To address this generalization issue, we introduce a dynamic Robustness Simulation Layer within the training pipeline. This layer integrates multiple attack modes and functions as a strong regularization term through a probabilistic triggering mechanism.

First, considering that practical EEG analysis and processing typically concentrate on specific frequency bands, we enforce a strict Band-Pass Training Constraint. Specifically, the model is subjected to ideal band-pass filtering attacks that truncate all frequency components outside the target band. This constraint compels the Encoder to forgo utilizing ultra-low-frequency (drift) or ultra-high-frequency (EMG noise) regions which are susceptible to filtration and instead redundantly distribute information within the core frequency band of 4–40 Hz.

Second, to mitigate issues arising from sampling rate mismatches between different acquisition devices, we introduce a Physical Resampling Attack. By simulating the reduction and restoration of signal sampling rates via interpolation algorithms, we force the model-generated features to maintain invariance to temporal axis scaling. Specifically, the original EEG signal (sampled at 250 Hz) is aggressively downsampled to a target frequency of 80 Hz and subsequently upsampled back to its original length, effectively smoothing out high-frequency spatial details. To ensure uninterrupted gradient propagation during end-to-end training, this physical resampling process is implemented using fully differentiable linear interpolation as a substitute for traditional discrete re-sampling. Because linear interpolation merely applies linear combinations of adjacent data points, the loss gradients can backpropagate smoothly and precisely through the attack module to the encoder, thereby bypassing the need for approximation techniques such as Straight-Through Estimators (STEe).

Furthermore, we employ a Spectral Dropout strategy, which randomly zeros out contiguous frequency bands in the frequency domain to simulate burst spectral losses that may occur during transmission. During this attack, a continuous frequency block comprising exactly 30% of the entire frequency band is randomly selected and its amplitude is set to zero.

To balance extraction accuracy and host signal fidelity, these attacks are integrated using a dynamic, stage-based probabilistic triggering mechanism. In the initial survival training stage, the model is exposed exclusively to the resampling attack to build fundamental structural robustness. During the subsequent refinement stage, the attacks are applied probabilistically to each mini-batch: physical resampling is triggered with a 70% probability, band-pass filtering with 10%, and spectral dropout with 10%. The remaining

10% of the batches bypass the attack module entirely to ensure the network does not lose its precision on clean data. The combined application of these attack strategies exposes the model to various hostile environments during the training phase, thereby ensuring superior robustness during the inference phase.

3. Experiment

3.1. Dataset

This study utilizes two datasets: the BCI Competition IV 2a dataset (also known as the Graz-A dataset) [23] and the BCI Competition IV 2b dataset (also known as the Graz-B dataset). The first dataset comprises 22-channel electroencephalogram (EEG) and 3-channel electrooculogram (EOG) data collected from 9 subjects. The signals were sampled at 250 Hz and pre-processed with a 0.5–100 Hz band-pass filter. The experimental paradigm followed a cue-based four-class motor imagery task. Subjects participated in two recording sessions on different days. In each session, subjects performed motor imagery tasks involving the left hand, right hand, both feet, or tongue, guided by visual arrow cues displayed on a screen. Each session consisted of 288 trials. Each trial lasted approximately 6 s, with the motor imagery task duration being 4 s. The training data provided includes expert-labeled artifact information and class labels. Additionally, the second dataset, Graz data set B, contains 3-channel bipolar EEG (C3, Cz, and C4) and 3-channel EOG data from 9 subjects, focusing on a cue-based two-class motor imagery task involving the left and right hands. These signals were similarly sampled at 250 Hz and band-pass filtered between 0.5–100 Hz.

3.2. Loss Function

The training objective of the network is to identify an optimal equilibrium between reconstructing the watermark and minimizing host carrier distortion. To this end, we define a composite loss function consisting of two components.

The first component is the Reconstruction Loss, which quantifies the discrepancy between the extracted secret information and the original information. As this constitutes a binary classification problem, we employ the Binary Cross-Entropy (BCE) Loss to provide steep gradient guidance, thereby accelerating model convergence.

The second component is the Distortion Loss, which measures the similarity between the watermarked signal and the original host carrier. We utilize the Mean Squared Error (MSE) Loss to penalize the Euclidean distance between the two signals in the time domain, ensuring that the watermark embedding does not alter the fundamental waveform characteristics of the EEG. The total loss function is defined as follows:

$$L_{\text{total}} = \lambda_{\text{rec}} \times \text{BCE}(S, \hat{S}) + \lambda_{\text{dist}} \times \|C - C_{\text{stego}}\|^2 \tag{5}$$

where λ_{rec} and λ_{dist} represent the weighting factors for the reconstruction loss and distortion loss, respectively.

3.3. Implementation Details and Experimental Setup

In this study, all neural networks were implemented using the PyTorch 2.8.0 framework and trained on an NVIDIA RTX 5090 GPU. The Adam optimizer was employed with a batch size of 32. The initial learning rate was set to 0.00002, and the model was trained for a total of 600 epochs. The input consists of single-channel segments with 1000 sampling points, corresponding to 4 s of EEG activity. The dataset was partitioned into an 80% training set and a 20% validation set, ensuring strict separation to prevent data leakage. The training process was conducted in a two-stage manner: for the first 400 epochs, the weights for the reconstruction loss (λ_{rec}) and distortion loss (λ_{dist}) were set to 10 and 0.05, respectively; for the subsequent 200 epochs, both weights (λ_{rec} and λ_{dist}) were adjusted to 1. The loss curve

during the training process is shown in Figure 3. We selected PSNR and Bit Accuracy as the evaluation metrics. PSNR quantifies the imperceptibility of the watermark, while Bit Accuracy (BA) evaluates the model's capability to recover the embedded information.

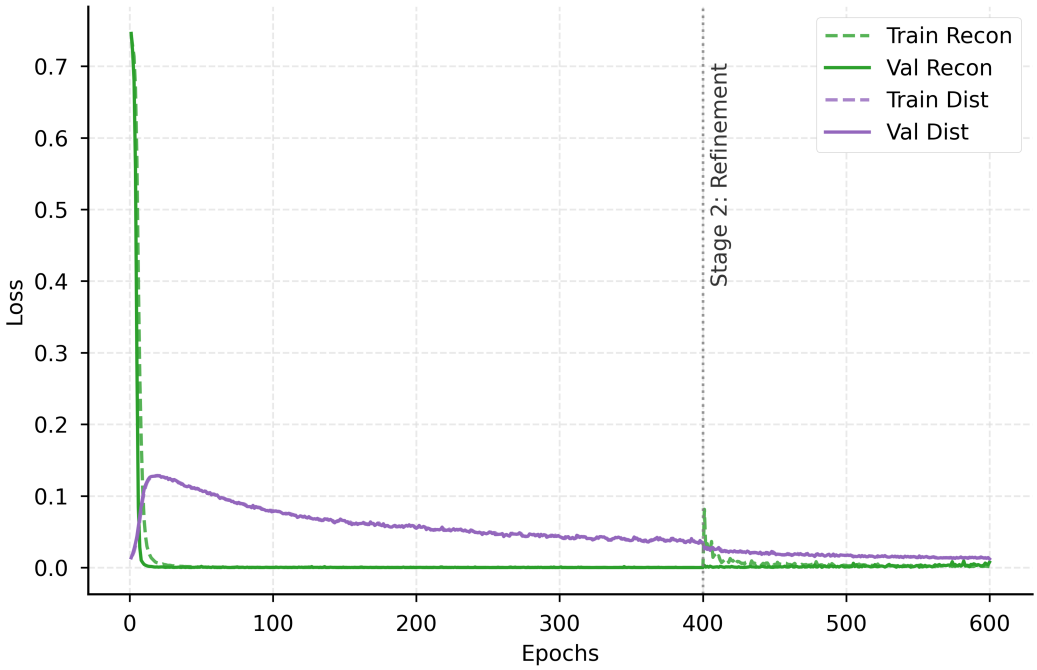

Figure 3. Loss Curve.

4. Results and Discussion

4.1. Performance Testing

The experimental results evaluating the model's performance on the Graz-A dataset are presented in Table 1. To ensure concise formatting, the attack scenarios in the table are abbreviated as follows: Clean (No attack), Noise (Gaussian noise with a variance of 0.1), Cr (Cropping at specified percentages), BP (4–40 Hz Band-pass filtering), Resamp (50% Resampling), and Gain (0.8× Amplitude Gain). These five specific channels (Fz, C3, Cz, C4, and Pz) were selected for evaluation because they represent the key functional cortical regions encompassing the frontal, central, parietal, and bilateral sensorimotor areas that are most critical for typical BCI tasks. As demonstrated in Table 1, the proposed DS-FTAN maintains high imperceptibility across all tested channels, with PSNR values ranging from 35.89 dB to 37.02 dB. Under the Clean scenario, the model achieves high decoding accuracy (99.99% to 100.00% with minimal standard deviations $\leq$ 0.02%). The model also demonstrates robust performance under various attack scenarios across different spatial locations. For instance, under high-intensity Gaussian noise (Noise), the watermark extraction accuracy remains above 95.47% for all channels. Even when the time-domain signal was subjected to severe 50% cropping (Cr-50%), the model successfully recovered between 87.26% and 89.03% of the watermark information. Furthermore, against the 4–40 Hz band-pass filtering (BP) commonly applied in clinical settings, the extraction accuracy across the five channels remains highly stable, ranging from 95.93% to 97.46%. Crucially, to validate the model's resilience against complex real-world transmission distortions, we additionally evaluated resampling and amplitude gain attacks. The model maintained excellent robustness, achieving an extraction accuracy between 97.73% and 98.92% under the 50% resampling attack (Resamp), and demonstrating good robustness ($\geq$99.99%) against the amplitude gain attack (Gain).

Table 1. Imperceptibility and robustness performance of the proposed DS-FTAN across five representative EEG channels under various attack scenarios (Results are reported as Mean ± SD across 5 random seeds).

Channel	PSNR (dB)	BA (%)							
		Clean	Noise	Cr-10%	Cr-30%	Cr-50%	BP	Resamp	Gain
Fz	36.31 ± 1.26	99.99 ± 0.01	96.96 ± 2.05	99.42 ± 0.23	95.43 ± 1.79	88.18 ± 2.99	96.87 ± 1.76	98.79 ± 0.91	99.99 ± 0.01
C3	36.33 ± 0.70	99.99 ± 0.01	95.79 ± 1.04	99.34 ± 0.09	95.17 ± 1.28	87.26 ± 2.06	95.93 ± 2.96	97.73 ± 1.27	99.99 ± 0.01
Cz	36.12 ± 1.05	99.99 ± 0.02	97.46 ± 1.28	99.55 ± 0.17	95.98 ± 1.51	88.97 ± 2.87	97.46 ± 1.94	98.92 ± 0.92	99.99 ± 0.01
C4	35.89 ± 1.42	99.99 ± 0.00	97.35 ± 1.08	99.55 ± 0.20	95.95 ± 1.93	89.03 ± 3.51	96.71 ± 2.70	98.59 ± 1.21	99.99 ± 0.01
Pz	37.02 ± 0.68	100.00 ± 0.00	95.47 ± 0.41	99.38 ± 0.13	95.11 ± 1.28	87.57 ± 2.31	97.44 ± 2.13	98.86 ± 0.81	100.00 ± 0.00

To intuitively demonstrate the imperceptibility of the proposed DS-FTAN framework indicated by the PSNR metrics, we visualize the physical waveform consistency in Figure 4. As illustrated in the global time-domain signal (Figure 4a), the morphological trajectory of the watermarked signal closely aligns with the original host EEG. The local zoom-in views detail the model's fidelity under varying signal dynamics. During both high-amplitude transient peaks (Figure 4b) and high-frequency rhythmic oscillations (Figure 4c), our residual generation strategy bounds the embedding perturbations to a microvolt level.

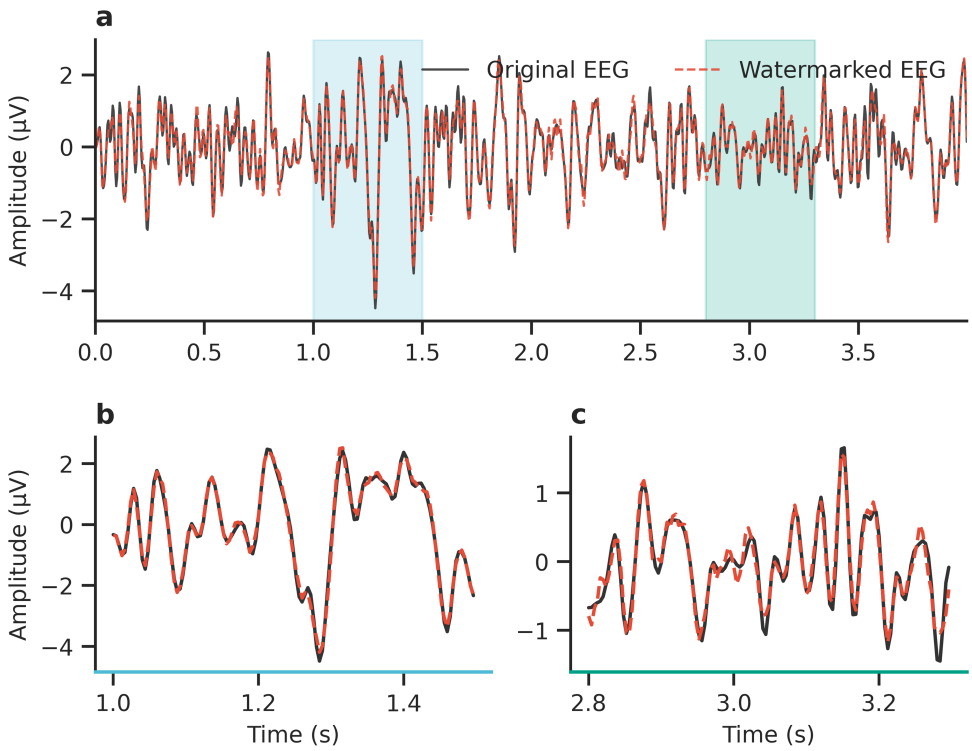

Figure 4. Time-domain waveform comparison between the original host EEG and the watermarked EEG generated by DS-FTAN: (**a**) the global time-domain signal; (**b**) local zoom-in view detailing high-amplitude transient peaks; (**c**) local zoom-in view detailing high-frequency rhythmic oscillations.

As shown in Table 2, we benchmarked the proposed DS-FTAN against a variety of existing watermarking schemes on the same dataset. To ensure a comprehensive and fair comparison, the baselines include both recent deep learning-based models and traditional methods (e.g., DWT-SVD-based approaches). Specifically, the performance metrics for Hidden, Dual, and RPW-EEG are directly cited from [21], evaluated under identical dataset and attack settings. Because the original literature provided bit accuracy (BA) to two decimal places, we appended zeros for formatting consistency. The empty entries in the Crop (50%) column indicate that this specific attack was not evaluated in their original study. The

other six baselines were strictly re-implemented and tested under identical experimental conditions, specifically utilizing the Fz channel for evaluation. Although methods such as RPW-EEG provide a foundational level of protection, they exhibit pronounced limitations regarding imperceptibility, evidenced by a Peak Signal-to-Noise Ratio of 25.26 decibels, as well as extraction accuracy under attack conditions. Conversely, traditional methods like LSB and Quantization achieve mathematically extremely high PSNR values (108.09 dB), but their robustness is highly fragile. Particularly when subjected to high-intensity noise at a level of 0.1 and band-pass filtering attacks, the bit accuracy of RPW-EEG drops substantially to 61.00% and 69.00%, respectively, while LSB and Quantization drop to random guessing levels (around 50%). The fundamental cause of this vulnerability lies in the architectural design of RPW-EEG, which functions primarily as a watermarking network performing convolution operations exclusively on one-dimensional time-series data. Such a purely time-domain convolutional architecture is constrained by local receptive fields and struggles to capture global frequency dependencies.

Table 2. Comparison with other baseline methods.

Models	PSNR (dB)	BA (%)			
		No Attack	Noised (0.1)	Crop (50%)	Band Pass (4–40Hz)
Hidden [21]	21.16	83.00	47.00	-	55.00
Dual [21]	22.48	81.00	48.00	-	51.00
RPW-EEG [21]	25.26	89.00	61.00	-	69.00
LSB [24]	108.09	100.00	50.27	74.76	49.72
Quantization [24]	108.09	100.00	50.03	74.87	50.06
Patchwork [24]	27.38	100.00	86.70	74.59	61.38
DWT-SVD-QIM [25]	41.49	99.73	98.41	74.08	65.69
PEE-HS [9]	47.22	100.00	50.17	98.02	50.27
DWT-SVD-FA [26]	32.59	100.00	100.00	74.33	50.22
Ours (DS-FTAN)	35.32	100.00	98.77	90.57	95.15

Consequently, the generated watermarked signals become extremely fragile when confronting unavoidable clinical frequency-domain operations like band-pass filtering. Similarly, while some traditional methods excel in specific scenarios—such as PEE-HS achieving 98.02% accuracy under 50% cropping, or DWT-SVD-FA resisting noise perfectly—they uniformly suffer severe degradation under clinical band-pass filtering (typically dropping to around 50–65%). In contrast, our DS-FTAN effectively overcomes this architectural blind spot by synergistically modeling both the time and frequency domains. This approach not only achieves high signal fidelity with a Peak Signal-to-Noise Ratio of 35.32 decibels but also maintains comprehensive robustness across diverse attack modalities. Notably, when facing band-pass filtering attacks that severely degrade the performance of both time-domain models and traditional DWT-SVD algorithms, DS-FTAN sustains a high extraction accuracy of 95.15%. Simultaneously, it maintains a robust accuracy of 90.57% under severe 50% cropping and 98.77% under high-intensity noise. This outcome demonstrates the core value of our proposed adaptive spectral gating mechanism in enhancing the survivability of the model against intensive and multifaceted signal processing operations.

4.2. Cross-Channel Generalization Analysis

In practical medical monitoring and Brain–Computer Interface applications, electroencephalogram acquisition devices exhibit significant hardware heterogeneity [27]. Ranging from single-channel portable sleep monitoring headbands to 128-channel medical-grade high-density electroencephalogram caps, the spatial topological structures and channel quantities of the electrodes vary drastically. If a watermarking model relies heavily on

the time-domain morphology of specific channels, prohibitive retraining costs must be incurred when encountering signals from new devices, additional electrodes, or different brain regions. Such an unscalable design severely hinders the large-scale deployment of deep watermarking models within distributed Brain–Computer Interface ecosystems.

To evaluate scalability without retraining for specific channels, we assessed the cross-channel generalization of the DS-FTAN framework. A model optimized solely on the Fz channel of the Graz-A dataset was applied directly to unseen channels (C3, Pz, etc.) without fine-tuning and compared against models utilizing Channel-Specific Training.

As evidenced in the Table 3, DS-FTAN demonstrates high transferability. Despite distributional discrepancies, signal fidelity remained high; for instance, transferring from Fz to C3 yielded a PSNR of 34.60 dB, only marginally lower than the 36.19 dB achieved by the channel-specific model. This suggests the model learns a universal perturbation strategy rather than overfitting to specific noise patterns. Crucially, extraction accuracy in No Attack scenarios remained close to 100%, validating the channel invariance of the dual-stream attention features.

Table 3. The results of cross-channel generalization.

Models	PSNR (dB)	BA (%)			
		No Attack	Noised (0.1)	Crop (50%)	Band Pass
Fz	35.32	100.0	98.77	90.57	95.15
C3	34.60	100.0	98.92	90.21	94.71
Cz	35.23	100.0	98.95	90.54	95.14
C4	34.90	99.9	98.74	90.61	95.02
Pz	35.42	100.0	98.81	91.81	95.40

Robustness metrics indicate that generalization persists even under complex attacks. While the cross-channel model showed slight performance degradation under high-intensity conditions (e.g., a $<3\%$ accuracy drop under band-pass filtering on Pz), it remained within acceptable limits. Notably, against severe 50% cropping attacks, accuracy consistently exceeded 90%, comparable to, and occasionally surpassing, channel-specific baselines.

Such significant zero-shot transferability indicates that the DS-FTAN model successfully captures the commonalities in global spectral distributions shared across brain regions during neural activities. This characteristic endows DS-FTAN with significant value for practical engineering implementation. In real-world cloud-based medical diagnostics or BCI data streaming scenarios, these preliminary transferability results suggest that the model has the potential to be further developed into a general-purpose foundational security module. It paves the way for future exploration into integrating such frameworks into the firmware of specific EEG devices or edge computing nodes. Although currently evaluated on a limited subset of channels, this cross-channel capability indicates that future iterations of DS-FTAN could potentially reduce the need for laborious fine-tuning across certain device configurations, offering a step towards standardized copyright verification. This not only reduces system deployment costs but also offers a promising solution for constructing heterogeneous, interconnected, and secure next-generation distributed medical monitoring networks.

4.3. Ablation Studies

To validate the necessity of the dual-stream architecture within the proposed DS-FTAN module, we conducted comprehensive ablation studies on the Graz-A dataset. We constructed two degraded baseline models: one removing the frequency-domain gating branch (retaining only the time-domain path) and another removing the time-domain path (retaining only the

frequency-domain branch). We compared the performance of these baseline models against the complete model across five representative channels (Fz, C3, Cz, C4, Pz).

The experimental results, presented in Tables 4–6, demonstrate the synergistic role of both temporal and frequency modeling in enhancing signal fidelity and robustness against specific attacks.

Table 4. Performance of the model excluding the frequency-domain gating branch.

Models	PSNR (dB)	BA (%)			
		No Attack	Noised (0.1)	Crop (50%)	Band Pass
Fz	31.14	100.0	99.96	91.27	91.21
C3	30.65	99.97	99.94	90.64	90.83
Cz	31.22	99.92	99.90	90.98	91.58
C4	30.89	99.99	99.91	91.16	91.52
Pz	31.54	99.99	99.97	91.20	91.71

Table 5. Performance of the model excluding the time-domain path.

Models	PSNR (dB)	BA (%)			
		No Attack	Noised (0.1)	Crop (50%)	Band Pass
Fz	36.44	99.97	93.24	85.78	94.56
C3	36.49	99.99	93.19	85.50	92.21
Cz	37.14	99.99	91.04	84.56	93.82
C4	36.26	99.97	92.49	84.56	93.92
Pz	37.25	100.0	92.09	85.58	93.32

Table 6. Full model performance.

Models	PSNR (dB)	BA (%)			
		No Attack	Noised (0.1)	Crop (50%)	Band Pass
Fz	35.32	100.0	98.77	90.57	95.15
C3	36.19	100.0	94.68	87.53	97.35
Cz	36.95	99.99	93.62	86.52	96.88
C4	35.96	99.99	96.18	90.09	98.14
Pz	36.45	99.99	95.84	89.59	94.71

Regarding signal imperceptibility, introducing the frequency-domain gating mechanism resulted in a significant PSNR improvement. The complete model and the pure frequency-domain baseline both maintained stable PSNR values between 35.32 dB and 37.25 dB across all tested channels, whereas the time-only baseline saw its PSNR values drop to the 30.65–31.54 dB range, indicating a difference of approximately 5 dB.

In terms of robustness against bandpass filtering attacks, the complete model demonstrated a clear advantage over the time-only baseline. When subjected to a severe 4–40 Hz bandpass filtering attack, the time-only baseline's extraction accuracy generally hovered around 90% to 91% across the channels (e.g., 90.83% for the C3 channel). In contrast, with the introduction of the dual-stream module, the complete model's accuracy under the same attack jumped to over 95%, reaching 97.68% on the C3 channel and 98.14% on the Pz channel.

The data indicates that the time-only baseline achieved slightly higher accuracy under noise (Noise 0.1) and partial cropping attacks compared to the complete model (typically within a 1–2% difference); however, this was accompanied by significantly reduced signal quality. Crucially, the approximately 5 dB decrease in PSNR serves as a direct quantitative measure of perturbation energy, revealing that the pure time-domain architecture achieves this marginal robustness gain by injecting substantially more global unstructured noise into the host signal, thereby violating the imperceptibility constraint re-

quired for clinical EEG. Conversely, while the frequency-only baseline (Table 5) maintained high PSNR, it suffered notable performance degradation under temporal distortions like 50% cropping (84.56–85.78%) and bandpass filtering (92.21–94.56%) compared to the full model. This confirms that the time-domain path is indispensable for anchoring local transient morphologies. Ultimately, the synergistic dual-stream framework achieves an optimal Pareto balance, strictly preserving signal imperceptibility while maintaining superior comprehensive robustness.

This indicates that pure time-domain convolutional architectures, lacking explicit modeling of frequency-domain features, tend to trade host signal quality for robustness by increasing the global noise intensity. In contrast, DS-FTAN intelligently identifies and leverages high-energy masking regions within the EEG spectrum for embedding, thereby achieving higher-capacity steganography without compromising the original waveform.

To further visualize and interpret the specific frequency bands selected by the adaptive Spectral Gating Mechanism, we extracted the internal gating weights from the pre-trained DualStreamBlock layers and analyzed the Power Spectral Density (PSD) of the generated watermark perturbations. As illustrated in Figure 5, the model's frequency masking strategy exhibits interpretable, physics-aware characteristics.

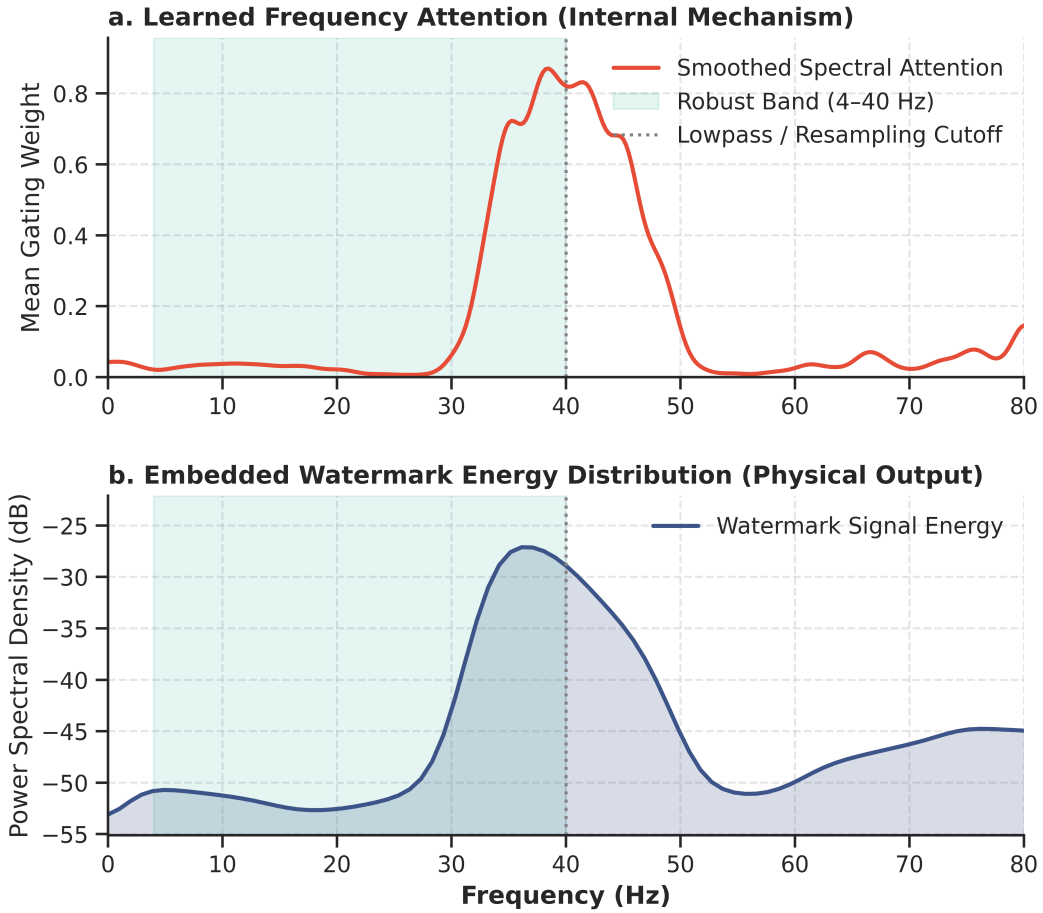

Figure 5. Frequency analysis of the Spectral Gating Mechanism. (**a**) The smoothed spectral attention weights extracted from the internal layers. (**b**) The Power Spectral Density (PSD) of the generated physical watermark signal.

Figure 5a reveals that the internal spectral attention places less emphasis on the low-frequency bands (0–30 Hz) and concentrates relatively higher weights in the 30–40 Hz region, followed by a significant decrease beyond 40 Hz. The physical PSD of the watermark

signal (Figure 5b) is highly consistent with this internal mechanism, with the embedded energy mainly concentrated within the robust band (4–40 Hz) and peaking around 35 Hz.

This frequency selection demonstrates an effective trade-off learned by the network. On the one hand, typical pristine EEG rhythms (e.g., Delta, Theta, and Alpha waves) possess high background energy in the 0–30 Hz range. Embedding a recognizable watermark in these bands would require higher absolute perturbation amplitudes, subsequently increasing the Mean Squared Error (MSE) and violating the imperceptibility constraint ($PSNR > 36$ dB). On the other hand, to survive the simulated clinical signal processing attacks, the model reduces watermark energy beyond 40 Hz to minimize the severe attenuation caused by clinical low-pass filtering and physical resampling operations. Consequently, the 30–40 Hz region—a band with relatively lower natural host energy that resides below the filtering cutoff—serves as a suitable band to achieve a sufficient local signal-to-noise ratio with minimal perturbation. This visualization indicates that the performance of DS-FTAN relies on an adaptive utilization of physiological spectral dynamics.

4.4. Downstream BCI Task Utility Evaluation

To evaluate the potential impact of the watermark embedding process on downstream brain–computer interface (BCI) task performance, we conducted utility experiments using the BCI Competition IV-2b dataset. This experiment utilized three core sensorimotor channels (C3, Cz, C4) critical for motor imagery intention recognition, providing a highly challenging real-world scenario. We employed the widely validated EEGNet as the intention recognition classifier.

Specifically, we adopted a pooled (subject-independent) experimental protocol. The data from all 9 subjects in Sessions 1 and 2 were aggregated into a single training set, and Session 3 from all subjects was combined into a single test set. This pooled regimen was selected to incorporate inter-subject variability and evaluate the model in a generalized BCI deployment scenario. Because the classifier was tested on this globally pooled set, we reported the global classification accuracy and Kappa score, and thus cross-subject standard deviations are not applicable here. Subsequently, utilizing the pre-trained DS-FTAN encoder, we independently embedded random secret bitstreams into the three channels of the test set. The watermarked data was directly fed into the baseline EEGNet for evaluation without any fine-tuning or retraining of the classifier.

The experimental results are presented in Table 7. The baseline classification accuracy for clean EEG signals was 70.81% (Kappa: 0.4163). After the blind embedding of the DS-FTAN watermark, the classification accuracy for the watermarked signals was 70.39% (Kappa: 0.4078). This comparison indicates that the accuracy degradation caused by watermark embedding was merely 0.42%. This negligible performance loss of only 0.42% provides strong evidence that the watermark perturbation does not alter the critical spatial and temporal topological structures of the EEG data, rendering it negligible in practical clinical and engineering applications. The underlying reason for this success lies in the unique residual generation strategy and dual-stream frequency–time fusion of DS-FTAN. The proposed spectral gating mechanism avoids causing structural distortions by strictly confining the embedded energy within redundant and secure physiological bands. This ensures that the watermark appears to the classifier as acceptable natural background noise, distributed redundantly and uniformly across the effective frequency bands of EEG channels.

Table 7. Impact of DS-FTAN Watermarking on Downstream BCI Motor Imagery Classification.

Data Modality	Channels	Accuracy (%)	Kappa Score
Original Clean EEG	C3, Cz, C4	70.81	0.4163
Watermarked EEG	C3, Cz, C4	70.39	0.4078

4.5. Discussion and Limitations

Our experimental results demonstrate that the proposed DS-FTAN framework achieves a balance between imperceptibility (PSNR > 36 dB) and robustness, significantly outperforming pure time-domain baselines such as RPW-EEG. This superiority is particularly evident under clinical band-pass filtering attacks. The fundamental reason for this success lies in our adaptive Spectral Gating Mechanism. Unlike conventional CNNs that struggle to capture global frequency dependencies due to their limited local receptive fields, our dual-stream architecture explicitly models the spectral distribution. By adaptively allocating watermark energy into robust, high-energy physiological bands and actively circumventing fragile ultra-low- or high-frequency regions, the model realizes high-capacity steganography without distorting the intrinsic morphological characteristics of the host EEG waveform. It is important to note that the zero-shot cross-channel generalization demonstrated in this study is currently validated only within BCI-relevant sensorimotor cortical regions (e.g., C3, Cz, C4). Given the inherent differences in physiological rhythm distributions across distinct brain areas, such as the occipital lobe, the model's universal generalization capability across whole-brain channels remains an important direction for future exploration.

Furthermore, the zero-shot cross-channel generalization capability demonstrated by DS-FTAN highlights its significant potential for real-world deployment. In distributed Brain–Computer Interface (BCI) ecosystems and remote telemedicine, hardware heterogeneity—ranging from single-channel consumer headbands to high-density medical caps—is a major bottleneck. Our findings indicate that DS-FTAN successfully extracts universally applicable spectral perturbation strategies rather than overfitting to specific electrode noise patterns. This characteristic highlights its potential to eventually serve as an adaptable copyright protection module for specific EEG applications, which could help mitigate the substantial computational costs associated with subject-specific retraining.

Despite these promising outcomes, several limitations must be acknowledged. First, while the watermarking process strictly preserves downstream task utility—evidenced by a minimal 0.42% accuracy drop in EEGNet intention recognition—the current validation is confined to sensorimotor rhythm-based motor imagery tasks. The potential impact of embedded perturbations on more fine-grained clinical diagnostic tasks, such as automated seizure detection or precise sleep staging, requires further rigorous clinical validation. Second, the introduction of the dual-stream architecture and FFT operations inevitably introduces higher computational overhead compared to lightweight single-stream networks. This increased complexity may pose latency challenges when deploying the extractor module on ultra-low-power edge computing nodes in portable BCI systems.

5. Conclusions

In this study, we proposed the Dual-Stream Frequency–Time Attention Network (DS-FTAN) to address the critical challenges of copyright protection and privacy in Brain–Computer Interface (BCI) data sharing. The existing deep learning watermark scheme is usually limited to single-domain modeling, so it often shows vulnerability in the face of frequency domain attacks, and it is difficult to maintain stable robustness among different subjects. In order to break through these limitations, DS-FTAN introduced a

dual-stream architecture to process spectrum and time characteristics in parallel. By integrating the adaptive spectrum gating mechanism, the model can strategically allocate watermark energy to strong robust frequency bands (especially in the 4–40 Hz range) for information embedding.

In summary, DS-FTAN provides highly practical technical support for building a secure and reliable distributed EEG data sharing system. Future work will be committed to exploring combined graph convolutional networks (GCNs) to optimize spatial topology modeling and introducing a federal learning framework to further strengthen the level of privacy protection in larger-scale BCI networks.

Author Contributions: Conceptualization, C.X. and L.Z.; methodology, W.Z., T.D. and C.X.; software, W.Z. and T.D.; validation, W.Z., T.D. and J.L.; formal analysis, T.D.; investigation, W.Z. and C.X.; resources, L.Z. and J.W.; data curation, W.Z. and J.L.; writing—original draft preparation, C.X.; writing—review and editing, D.D.; visualization, J.L.; supervision, L.Z., J.W. and D.D.; project administration, L.Z.; funding acquisition, L.Z. and J.W. All authors have read and agreed to the published version of the manuscript.

Funding: This research was funded by the Fundamental Research Funds for the Central Universities, China (3282025047, 3282024051, 3282024009).

Institutional Review Board Statement: Ethical review and approval were waived for this study, as it involved the secondary analysis of publicly available, fully anonymized datasets (Graz A and Graz B from BCI Competition IV).

Informed Consent Statement: Informed consent was obtained by the original investigators who collected the Graz A and Graz B datasets prior to their public release. For this secondary analysis, further participant consent was waived as the data are completely anonymized.

Data Availability Statement: Publicly available datasets were analyzed in this study. This data can be found here: https://bbci.de/competition/iv/download/ (accessed on 15 November 2025).

Conflicts of Interest: The authors declare no conflicts of interest.

References

1. Ma, W.; Zheng, Y.; Li, T.; Li, Z.; Li, Y.; Wang, L. A comprehensive review of deep learning in EEG-based emotion recognition: Classifications, trends, and practical implications. *PeerJ Comput. Sci.* **2024**, *10*, e2065. [CrossRef] [PubMed]
2. Liu, X.; Wang, W.; Liu, M.; Chen, M.; Pereira, T.; Doda, D.; Ke, Y.-F.; Wang, S.-Y.; Wen, D.; Tong, X.-G.; et al. Recent applications of EEG-based brain-computer-interface in the medical field. *Mil. Med. Res.* **2025**, *12*, 14. [PubMed]
3. Pulido-Gaytan, B.; Tchernykh, A.; Cortés-Mendoza, J.M.; Babenko, M.; Radchenko, G.; Avetisyan, A.; Drozdov, A.Y. Privacy-preserving neural networks with Homomorphic encryption: Challenges and opportunities. *Peer-to-Peer Netw. Appl.* **2021**, *14*, 1666–1691. [CrossRef]
4. Xia, K.; Duch, W.; Sun, Y.; Xu, K.; Fang, W.; Luo, H.; Zhang, Y.; Sang, D.; Xu, X.; Wang, F.-Y.; et al. Privacy-preserving brain–computer interfaces: A systematic review. *IEEE Trans. Comput. Soc. Syst.* **2023**, *10*, 2312–2324.
5. Al-Aiash, I.; Alquran, R.; AlJamal, M.; Alsarhan, A.; Aljaidi, M.; Al-Fraihat, D. Optimized digital watermarking: Harnessing the synergies of Schur matrix factorization, DCT, and DWT for superior image ownership proofing. *Multimed. Tools Appl.* **2025**, *84*, 19817–19852.
6. Luo, H.; Li, L.; Li, J. Digital watermarking technology for AI-generated images: A survey. *Mathematics* **2025**, *13*, 651. [CrossRef]
7. Awasthi, D.; Khare, P.; Srivastava, V.K. Internet of medical things-based authentication for an optimized watermarking of encrypted EEG. *J. Supercomput.* **2024**, *80*, 2970–3004.
8. Mekhfioui, M.; El Bazi, N.; Laayati, O.; Satif, A.; Bouchouirbat, M.; Kissi, C.; Boujiha, T.; Chebak, A. Optimized digital watermarking for robust information security in embedded systems. *Information* **2025**, *16*, 322. [CrossRef]
9. Bhalerao, S.; Ansari, I.A.; Kumar, A. Protection of BCI system via reversible watermarking of EEG signal. *Electron. Lett.* **2020**, *56*, 1389–1392. [CrossRef]
10. Raj, V.A.; Parupudi, T.; Thalengala, A.; Nayak, S.G. A comprehensive review of deep learning models for denoising EEG signals: Challenges, advances, and future directions. *Discov. Appl. Sci.* **2025**, *7*, 1268. [CrossRef]

11. Zhang, W.; Jiang, M.; Teo, C.K.A.; Bhuvanakantham, R.; Fong, L.; Sim, W.K.J.; Guo, Z.; Foo, C.H.V.; Chua, R.H.J.; Padmanabhan, P.; et al. Revealing the spatiotemporal brain dynamics of covert speech compared with overt speech: A simultaneous EEG-fMRI study. *NeuroImage* **2024**, *293*, 120629. [PubMed]
12. Amer, N.S.; Belhaouari, S.B. EEG signal processing for medical diagnosis, healthcare, and monitoring: A comprehensive review. *IEEE Access* **2023**, *11*, 143116–143142. [CrossRef]
13. Luo, Y.; Li, L.; Liu, J.; Tang, S.; Cao, L.; Zhang, S.; Qiu, S.; Cao, Y. A multi-scale image watermarking based on integer wavelet transform and singular value decomposition. *Expert Syst. Appl.* **2021**, *168*, 114272. [CrossRef]
14. Liu, J.; Huang, J.; Luo, Y.; Cao, L.; Yang, S.; Wei, D.; Zhou, R. An optimized image watermarking method based on HD and SVD in DWT domain. *IEEE Access* **2019**, *7*, 80849–80860. [CrossRef]
15. Baluja, S. Hiding images in plain sight: Deep steganography. *Adv. Neural Inf. Process. Syst.* **2017**, *30*, 2066–2076.
16. Mareen, H.; Antchougov, L.; Van Wallendael, G.; Lambert, P. Blind deep-learning-based image watermarking robust against geometric transformations. In Proceedings of the IEEE International Conference on Consumer Electronics (ICCE), Las Vegas, NV, USA, 6–8 January 2024; pp. 1–2.
17. Zhao, Y.; Wang, C.; Zhou, X.; Qin, Z. DARI-Mark: Deep learning and attention network for robust image watermarking. *Mathematics* **2023**, *11*, 209.
18. Wang, B.; Wu, Y.; Wang, G. Adaptor: Improving the robustness and imperceptibility of watermarking by the adaptive strength factor. *IEEE Trans. Circuits Syst. Video Technol.* **2023**, *33*, 6260–6272. [CrossRef]
19. Zhang, X.; Li, R.; Yu, J.; Xu, Y.; Li, W.; Zhang, J. EditGuard: Versatile image watermarking for tamper localization and copyright protection. In Proceedings of the IEEE/CVF Conference on Computer Vision and Pattern Recognition (CVPR), Seattle, WA, USA, 17–21 June 2024; pp. 11964–11974.
20. Rahman, M.S.; Khalil, I.; Yi, X. Reversible biosignal steganography approach for authenticating biosignals using extended binary Golay code. *IEEE J. Biomed. Health Inform.* **2021**, *25*, 35–46. [PubMed]
21. Qin, T.; Yi, H.; Qian, J.; Jin, X.; Liu, H.; Kong, W. RPW-EEG: An unified framework for robust and practical watermark of EEG. In *Proceedings of the Annual Meeting of the Cognitive Science Society*; University of California: Berkeley, CA, USA, 2025; Volume 47. Available online: https://escholarship.org/uc/item/96h9c291 (accessed on 19 June 2026).
22. Dliou, A.; Latif, R.; Laaboubi, M.; Maoulainine, F.; Elouaham, S. Noised abnormal ECG signal analysis by combining EMD and Choi-Williams techniques. In Proceedings of the IEEE International Conference on Complex Systems (ICCS), Agadir, Morocco, 5–6 November 2012; pp. 1–5.
23. Tangermann, M.; Müller, K.-R.; Aertsen, A.; Birbaumer, N.; Braun, C.; Brunner, C.; Leeb, R.; Mehring, C.; Miller, K.J.; Müller-Putz, G.R.; et al. Review of the BCI competition IV. *Front. Neurosci.* **2012**, *6*, 55. [CrossRef] [PubMed]
24. Kong, X.; Feng, R. Watermarking medical signals for telemedicine. *IEEE Trans. Inf. Technol. Biomed.* **2001**, *5*, 195–201. [CrossRef] [PubMed]
25. Trung, P.D.; Hai, N.N.; Ha, N.T.H. Secure EEG-based user authentication system integrated with robust watermarking. In *Proceedings of the 10th International Symposium on Information and Communication Technology*; Association for Computing Machinery: New York, NY, USA, 2019.
26. Gupta, A.K.; Chakraborty, C.; Gupta, B. Watermarking of EEG Data to Provide Security Based on DWT-SVD and Optimized by Firefly Algorithm. *Int. J. Distrib. Syst. Technol.* **2022**, *13*, 1–16. [CrossRef]
27. Bigdely-Shamlo, N.; Touryan, J.; Ojeda, A.; Kothe, C.; Mullen, T.; Robbins, K. Automated EEG mega-analysis I: Spectral and amplitude characteristics across studies. *NeuroImage* **2020**, *207*, 116361. [CrossRef] [PubMed]

Disclaimer/Publisher's Note: The statements, opinions and data contained in all publications are solely those of the individual author(s) and contributor(s) and not of MDPI and/or the editor(s). MDPI and/or the editor(s) disclaim responsibility for any injury to people or property resulting from any ideas, methods, instructions or products referred to in the content.